

## Airgap Prediction from Second-Order Diffraction and Stokes Theory

*Bert Sweetman and Steven R. Winterstein*

Civil and Environmental Engineering  
Stanford University, USA

*Trond Stokka Meling*

Statoil  
Stavanger Norway

### ABSTRACT

The airgap of a specific semi-submersible platform subjected to irregular waves is considered. Detailed model test results for both motions and airgap time histories are used to verify analysis results. The effects of various methods of including second-order diffraction contributions are demonstrated. A new method is proposed for use in post-processing second-order hydrodynamic transfer functions in which those transfer functions that are unavailable or believed to be unreliable are replaced with those of an undisturbed second-order Stokes wave.

**KEY WORDS:** offshore structures; semi-submersible; airgap; second-order diffraction; extreme values; model test results; Veslefrikk.

### INTRODUCTION AND BACKGROUND

Airgap modelling is of concern for both fixed and floating structures, but it is particularly challenging in the case of floating structures because of their large volumes and the resulting effects of wave diffraction and radiation. Standard airgap response prediction uses linear theory, which generally does not effectively reproduce measurements from model tests. First-order diffraction is considerably less demanding than second-order, so use of only first-order diffraction merits some consideration. Second-order diffraction effects are expected to better reflect observed data. However, these radiation/diffraction panel calculations are very sensitive to the numerical modelling.

The cost of increasing the airgap for a semi-submersible is considerably higher than that for a fixed structure. Hence, instead of increasing the still-water airgap, it may be less expensive to strengthen the underside of the deck to withstand rare negative airgap events. In order to know the wave load and where impact will occur, reliable prediction tools are important. Model tests are often performed as part of the design of a new semi-submersible. If so, these calculations are needed to determine the locations at which airgap probes should be placed on the model.

Here, the numerical impact of modelling second-order diffraction effects is assessed by comparing various predictions of the statistical behavior of the free surface with model test results. Diffraction results come from an industry-standard state-of-the-art computer program which applies second-order panel diffraction theory. All analysis and model test results presented here are relevant to the Veslefrikk semisubmersible, the plan view of which is shown in Fig. 1. Other relevant particulars for the vessel as analyzed include: draft: 23 m, displacement: 40,692 tonnes, airgap to still water level: 17.5 m and water depth on location: 175 m.

### AIRGAP NOTATION AND VESLEFRIKK MODEL

The airgap,  $a(t)$ , can be considered a linear combination of three terms:  $a_0$ , the still-water airgap distance,  $\eta(t)$ , the wave surface elevation at a particular location along the structure measured with respect to a fixed observer, and  $\delta(t)$  the corresponding vertical motion of the platform.

Among the various terms in the equation  $a(t) = a_0 - [\eta(t) - \delta(t)]$ , the vertical offset due to rigid body motion of the vessel,  $\delta(t)$ , is perhaps the most straightforward to model. Linear diffraction theory may often suffice to accurately model this offset. In contrast, the free surface elevation,  $\eta(t)$ , generally shows nonlinear behavior—and hence represents a non-Gaussian process. Modelling attention is therefore focused here on  $\eta(t)$ .

Specifically,  $\eta(t)$  is assumed to be a sum of incident and diffracted waves,  $\eta_i$  and  $\eta_d$ , each of which is a sum of first- and second-order components. This assumption is applied in the panel-diffraction analysis and is consistent with most state-of-the-art nonlinear hydrodynamic analyses, which generally employ second-order perturbation solutions.

Model test data used for verification of the hydrodynamic analysis come from a 1:45 length-scale model of Veslefrikk. Tests were performed in the wave tank at Marintek using various types of irregular waves (Fokk, 1995). Fig. 1 shows a plan view of the platform, together with the 9 locations for which the airgap responses have been measured as a function of time. Note that airgap probes with lower numbers are generally further up-stream, i.e., closer to the wave generator. All tests studied here apply long-crested waves travelling along the diagonal of the structure.

The relative airgap at each of the wave-probe locations and the platform rigid-body motions have been recorded. The rigid body motions permit calculation of the net vertical displacement,  $\delta(t)$ , at any field-point location  $(x, y)$ . This displacement is then subtracted from the measured airgap to determine the absolute wave elevation,  $\eta(t)$ , with respect to a fixed observer. The result is used for comparison

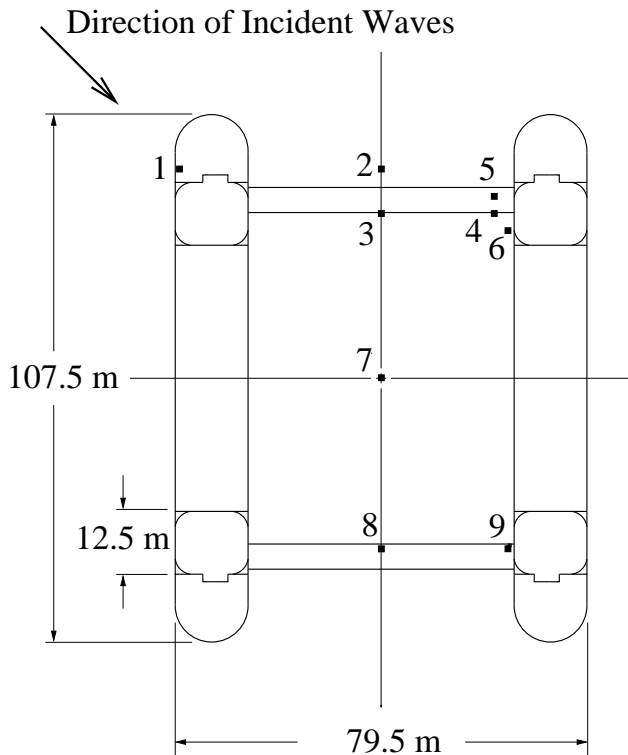


Fig. 1: Plan view of Veslefrikk platform and location of airgap probes.

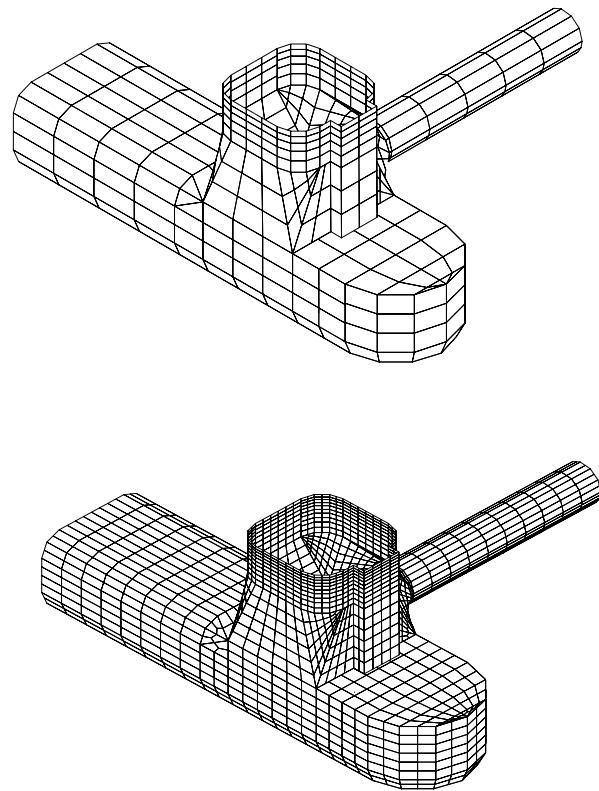


Fig. 2: Comparison of meshing options used in hydrodynamic analysis

with analytical predictions which assume a motionless structure.

## SECOND-ORDER DIFFRACTION ANALYSIS

A recognized industry-standard second-order panel diffraction program was used to analyze Veslefrikk. The semi-submersible is symmetric about each of its transverse and longitudinal axis. Fig. 2 shows both the coarse and fine numerical models, which were used in two separate analyses. The coarse model includes 524 panels in each quadrant, while the fine includes 2066.

The full second-order quadratic transfer functions (QTF's) covering  $n$  discrete frequencies,  $f_n$ , is an  $n \times n$  matrix of complex numbers, which can be represented as two separate  $n \times n$  matrices: one of magnitudes and one of phases. The magnitude and phase transfer function matrices for wave probe location 6 are shown in Fig. 3. These QTF's are typical of each of the nine airgap probes analyzed. Each intersection of the mesh on the figure represents a single term in the QTF matrix.

A more simplified representation of these transfer functions which is useful for comparison purposes can be made by considering only the on-diagonal terms of the matrix, i.e. only those terms  $H_2^+(f_1, f_2)$  for which  $f_1 = f_2$ . Fig. 4 is such a representation, with abscissa  $t_1 = t_2$ , where  $t_1 = 1/f_1$  and  $t_2 = 1/f_2$ . On Fig. 4, the line marked "Stokes Theory" represents the QTF implied by Stokes' second-order wave theory only, and does not consider any diffraction effects associated with the presence of the structure. The results denoted "Diffraction: Fine Mesh" arise from the finer of the two meshes which is presented in Fig. 2 and the "Diffraction: Coarse Mesh" results are from the more coarse mesh. The hydrodynamic analysis with the more fine

physical mesh was also analyzed over a more fine set of frequencies in the range of interest ( $\Delta f = 0.0045$  Hz vs 0.01 Hz). It is apparent from these figures that the more coarse physical mesh had some effect on the QTF results at each frequency analyzed, and that the finer frequency mesh captured frequency-dependent behavior which the coarser frequency mesh did not seek to evaluate. However, the mesh density did not have as large an effect on the QTF's as might have been expected, particularly in the short-period range.

The vertical scale of the first plot in Fig. 4 is a linear scale which has been truncated at  $|H_2^+(t_1, t_2)| = 0.3$  to show the detailed behavior of the QTF diagonals. At very low periods the QTF magnitudes grow considerably larger for all field-point locations. The second plot in Fig. 4 is a repeat of the first, except that the vertical axis is replaced with a logarithmic scale and the horizontal axis is extended to periods as low as 4 s. At location 6,  $|H_2^+(t_1, t_2)|$  for the coarse mesh reaches a maximum of 27; excessively large QTF's at high frequencies were observed for all nine field-point locations. Inclusion of these large QTF values at low-periods yields dramatic overestimation of response amplitude relative to model test results, as will be shown later.

## STATISTICAL AIRGAP PREDICTION

The diffraction results, as presented in Figures 3 and 4, are used in conjunction with a specified seastate to directly calculate the statistics of the airgap response. For all results presented here, the seastate is bimodal with  $H_s = 12$  m,  $T_p = 11.5$  s., and equivalent steepness

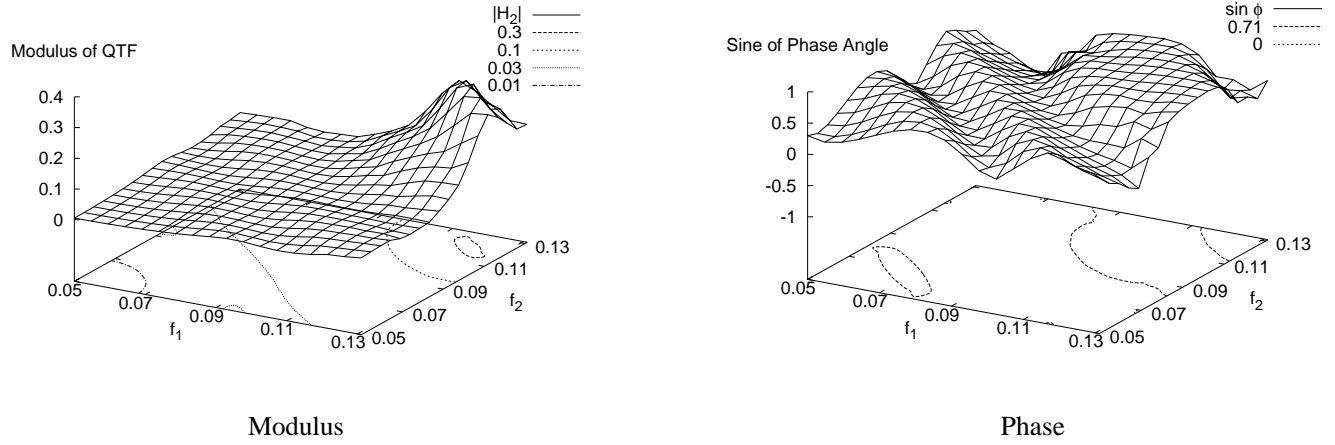


Fig. 3: Modulus and phase of second-order quadratic transfer functions from diffraction (location 6, typical)

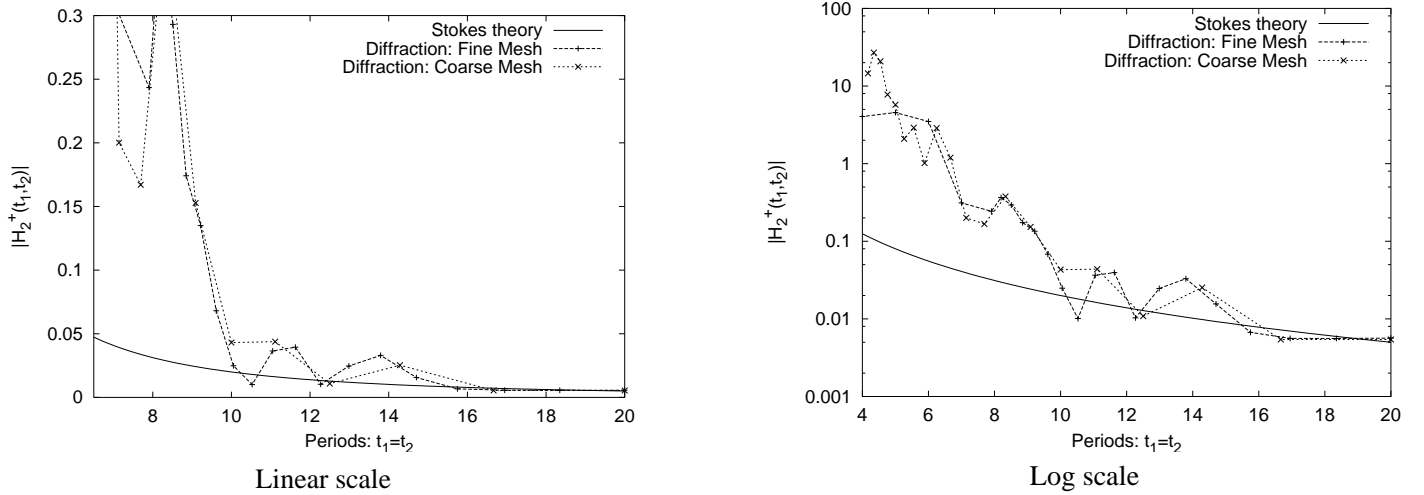


Fig. 4: Diagonals of quadratic transfer function matrix from diffraction (location 6, typical)

parameter  $\gamma = 4.0$ . The first four statistical moments are calculated using the methods originated by Kac and Siebert (1947) and later expanded by Næss. The first- and second-order processes  $\eta_1(t)$  and  $\eta_2(t)$  are rewritten in terms of standard Gaussian processes:

$$\eta_1(t) = \sum_{j=1}^{2n} c_j u_j(t); \quad \eta_2(t) = \sum_{j=1}^{2n} \lambda_j u_j^2(t) \quad (1)$$

in which  $n$  is the number of frequency components of  $\eta_1(t)$ .

The coefficients  $c_j$  and  $\lambda_j$  can be obtained by solving an eigenvalue problem of size  $n$  for problems involving difference or sum frequencies only (Næss, 1986, Næss, 1992). Problems such as these, which involve both sum and difference frequencies, lead to eigenvalue problems of size  $2n$ , twice the number of frequency components of  $\eta_1(t)$ . Implementation of the theory is described in Winterstein et al., 1994, with extensions to airgap analysis from Manuel and Winterstein, 2000.

The resulting moments of  $\eta$  can be found directly from the coefficients  $c_j$  and  $\lambda_j$ :

$$\sigma_{\eta}^2 = \sum_{j=1}^{2n} (c_j^2 + \lambda_j^2) \quad (2)$$

$$\alpha_{3,\eta} = \frac{1}{\sigma_x^3} \sum_{j=1}^{2n} (6c_j^2 \lambda_j + 8\lambda_j^3) \quad (3)$$

$$\alpha_{4,\eta} = 3 + \frac{1}{\sigma_x^4} \sum_{j=1}^{2n} (48c_j^2 \lambda_j^2 + 48\lambda_j^4) \quad (4)$$

This method of direct statistical calculation is used to produce the statistical moment results shown in Figures 5 and 6. The plot of peaks is calculated as follows: The expected maximum of a standard Gaussian process in  $N$  cycles (e.g., Crandall and Mark, 1963) is first determined. The Hermite model (e.g., Winterstein, 1988) is then applied using the theoretical skewness ( $\alpha_{3,\eta}$ ) and kurtosis ( $\alpha_{4,\eta}$ ) estimates from the Equations 3 and 4 to transform this Gaussian maximum to predict the non-Gaussian extreme value. Results presented here use an optimization routine to minimize error in matching skewness and kurtosis values. These analytical results predict mean 3-hour maxima, which are compared with average maxima over 5 separate 3-hour model tests.

Recall from the discussion of Fig. 4 that the QTF's resulting from diffraction grow exceedingly large at low periods. Post-processing the complete set of QTF's leads to dramatic over-prediction of the standard deviation and expected maxima of the response for all nine airgap probe locations, as shown in Fig. 5. Results based on the coarse

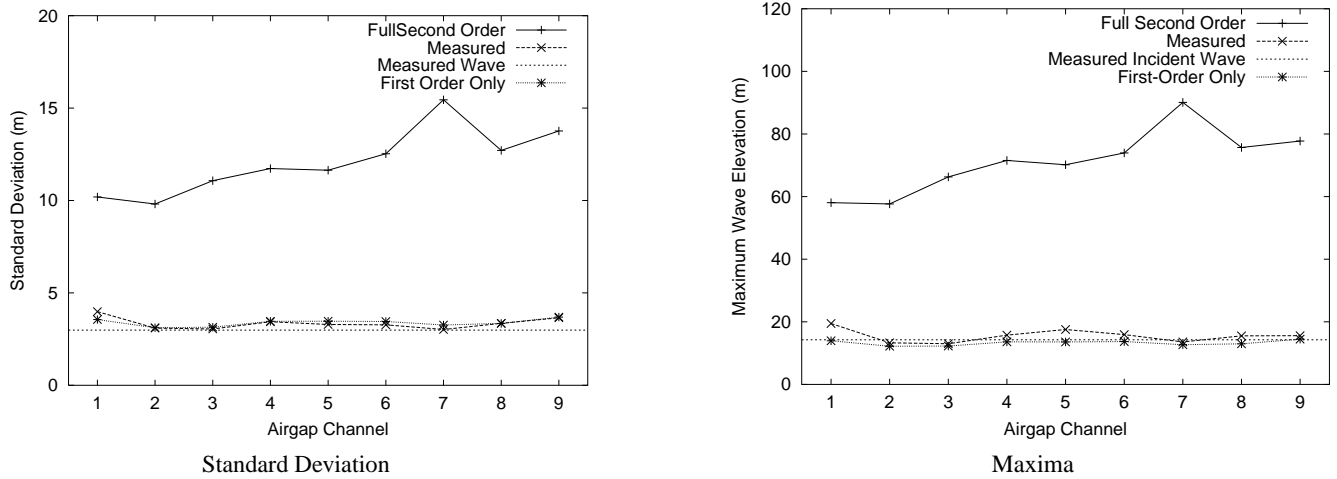


Fig. 5: Predictions based on use of complete second-order transfer functions

mesh model were selected for use in Fig. 5 because that diffraction analysis was completed over a broader period range: the complete QTF matrix was calculated to periods as low as 4 s.

The results presented in Figure 5 are clearly inaccurate and would not be at all useful for design. The dramatic over-prediction is believed to be due to over-prediction of true second-order effects at high frequencies. It is hypothesized that improved prediction results can be obtained by using the diffraction QTF's only over the range for which they appear reasonable: in this case, periods greater than about 8 s. Fortunately, the peak of the input wave spectrum is well within this period range for these model tests.

For periods less than a cut-off period,  $T_c$ , of about 8 s., the diffraction QTF's are not used. Simply zeroing-off the unused QTF's would be straight-forward, but the actual QTF's below  $T_c$  are believed to be non-zero. Somehow extrapolating those QTF's believed to be reasonable may be another possibility, but the details of a valid QTF extrapolation may be somewhat arbitrary. QTF's as predicted from Stokes theory have several properties that make them a reasonable substitution for unusable QTF's predicted by diffraction.

Stokes theory is well known and the QTF's can be calculated analytically. Stokes QTF's have previously been applied in conjunction with linear diffraction results over the entire frequency range (Sweetman and Winterstein, 2001). It was found that this combination results in better predictions of the maximum water surface elevation than does use of the linear diffraction results alone. It is recognized that Stokes transfer functions ignore diffraction effects, which are potentially most important for small period waves. However, they are used here since reliable prediction of diffraction effects is not available.

In the present analysis, Stokes QTF's were substituted for the diffraction QTF if the average of the frequency pair,  $\frac{1}{2}(f_1 + f_2)$ , is greater than a cut-off frequency,  $f_c = 1/T_c$ . The selection of this form for the cut-off will be discussed later. Cut-off periods of  $T_c = 7, 8$  and  $9$  s. each have been applied, and the results are compared in Fig. 6. "Coarse Mesh above 7 sec" noticeably over-predicts at all locations. This observed over-prediction, relative to  $T_c = 8$  or  $9$  s. and to measured data, confirms that the diffraction results should not be trusted for periods as low as 7 s. for this structure.

As can also be observed in the figure, second-order diffraction has only a minor effect on the standard deviation, i.e. the rms response of the process. It appears that linear diffraction alone (calculated here

using the fine mesh) may be sufficient to accurately predict the rms level of the wave elevation, and hence that of the airgap response. However, the values of the coefficients of skewness and kurtosis both deviate substantially from their respective Gaussian values of 0 and 3.

The non-Gaussian effects associated with increased values of the coefficients of skewness and kurtosis substantially increases the prediction of the mean maximum from the "First-Order Only" result to approximately that of the observed model test data ("Measured"). The magnitude of the predicted peak is generally centered amongst the measured data. However, even these second-order predictions fail to adequately follow the trend in observed extremes at near-column locations. The discrepancy is particularly severe at locations 1, 5 and 9. At these locations, a run-up effect is expected to be important, and this is an effect which is not handled by the present analysis. Locations 4 and 6 will also have some influence of run-up.

Ignoring the  $T_c = 7$  s. results, comparable results are obtained from the second-order analysis using  $T_c$  equal to either 8 or 9 s., with either the coarse or fine mesh. Each of these analyses yields about the same level of agreement with the measured data. In particular, considering the mean maximum predicted airgap response, there is almost no difference between results for the coarse and fine meshing options for frequencies above 9 s., and only relatively slight differences between these results and those for the fine mesh above 8 s. Thus, results are not found to be particularly sensitive to the mesh density. As long as the very low period QTF's were not used ( $T_c < 8$  s.), all prediction results, regardless of modeling assumptions, show better agreement with measured data than results based on first-order alone. This finding suggests second-order diffraction applied over a limited period range captures important physical effects.

## CONCLUSIONS

A semisubmersible production platform, the Veslefrikk, has been analyzed using an industry-standard second-order hydrodynamic panel-diffraction computer program to predict quadratic transfer functions of the free surface.

Second-order diffraction was found to yield considerably better peak predictions than first-order alone. Predictions of mean maxima were typically 20% higher than those based on first order only. As part of post-processing the diffraction results, a new method has

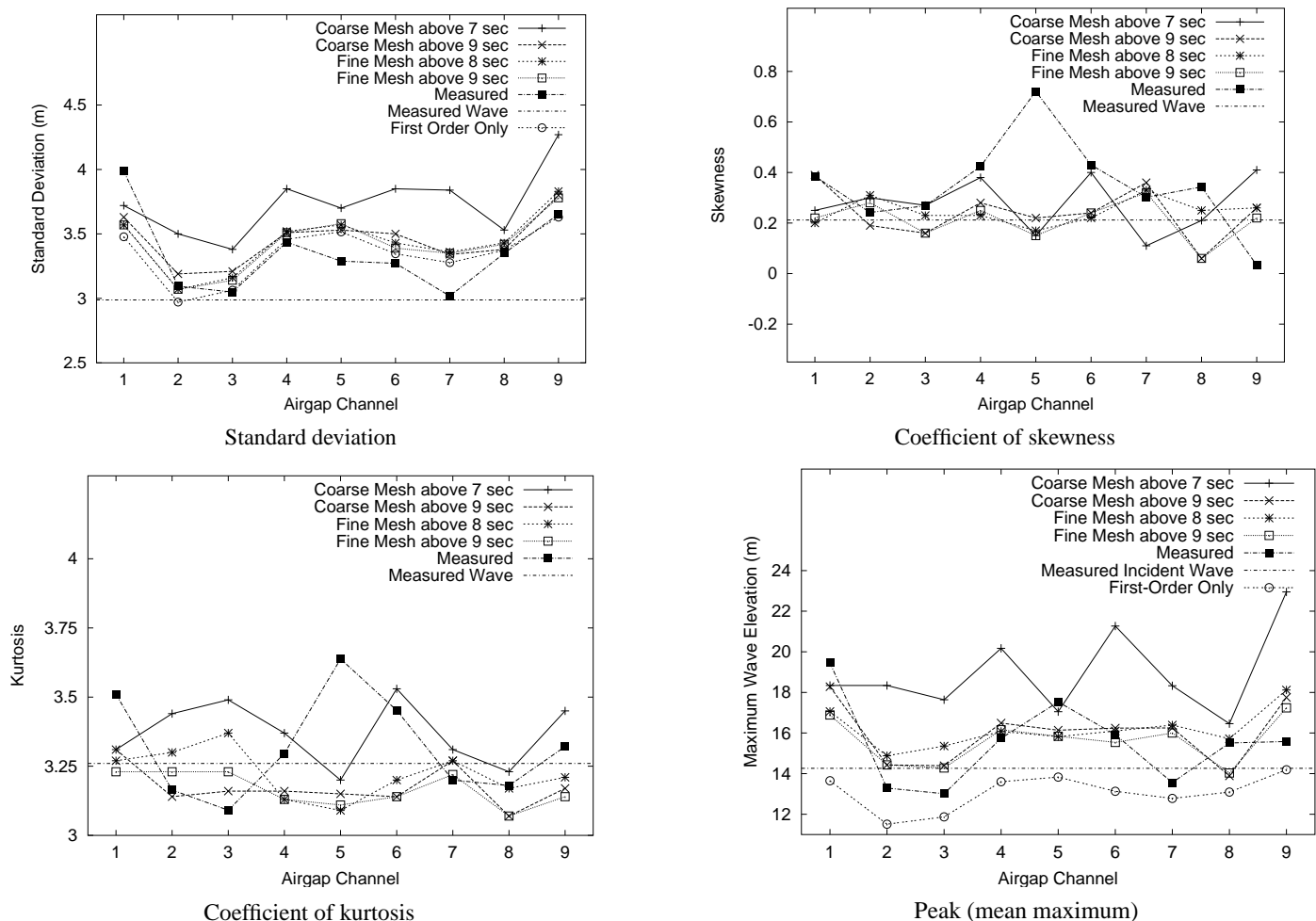


Fig. 6: Results based on using second-order diffraction transfer function results with Stokes second order transfer functions for low periods.

been introduced by which unknown high-frequency QTF's are approximated by those predicted by Stokes wave theory. Two different mesh densities were applied to both the body and the free surface, and the hydrodynamic results were not found to be very sensitive to the mesh density or the maximum frequency above which second-order diffraction results are not considered.

As long as very high frequency QTF's are not used, all prediction results based on Second-order diffraction, regardless of modeling assumptions, show better agreement with measured data than results based on first-order alone. Thus, use of second-order diffraction should be considered in practical design work if the airgap response is believed to be a critical design quantity.

#### ACKNOWLEDGEMENTS

The authors gratefully acknowledge the support of the Reliability of Marine Structures (RMS) program at Stanford University.

#### REFERENCES

Crandall SH and Mark WD (1963). *Random Vibration in Mechanical Systems*, Monograph, Academic Press.  
 Fokk T (1995). "Veslefrikk B Air Gap Model Tests," *Tech. Rep. 512167.00.01*, MARINTEK Trondheim, Norway.

Kac M and Siegert AJF (1947). "On the theory of noise in radio receivers with square law detectors," *Journal of Applied Physics*, no. 18, pp. 383–400.  
 Manuel L and Winterstein SR (2000). "Reliability Based Predictions of a Design Air Gap for Floating Offshore Structures," in "Proceedings 8'th ASCE Conf. on Probabilistic Mechanics and Structural Reliability," ASCE.  
 Næss A (1986). "The Statistical Distribution of Second-Order Slowly-Varying Forces and Motions," *Applied Ocean Research*, vol. 8, pp. 110–118.  
 Næss A (1992). "Prediction of extremes related to the second-order, sum-frequency response of a TLP," in "Proc., 2nd Intl. Offshore Polar Eng.," ISOPE, pp. 436–443.  
 Sweetman B and Winterstein SR (2001). "Non-Gaussian Air Gap Response Models for Floating Structures," *ASCE Journal of Engineering Mechanics*. Submitted for Review.  
 Winterstein S (1988). "Nonlinear vibration models for extremes and fatigue," *Journal of Engineering Mechanics ASCE*, vol. 114, no. 10, pp. 1772–1790.  
 Winterstein SR, Ude TC, and Marthinsen T (1994). "Volterra Models of Ocean Structures: Extreme and Fatigue Reliability," *Journal of Engineering Mechanics*, vol. 120, no. 6, pp. 1369–1385.